CrossMark

Effect of Low Temperature on Electromagnetic Radiation from Soft PZT SP-5A Under Impact Loading

SUMEET KUMAR SHARMA [1,3,4] ASHOK KUMAR SIVARATHRI,[1]
VISHAL S. CHAUHAN,[1] and MICHAEL SINAPIUS[2]

1.—School of Engineering, Indian Institute of Technology Mandi, Kamand, Himachal Pradesh 175005, India. 2.—Technische Universität Braunschweig, 38106 Brunswick, Germany. 3.—e-mail: sumeet_sharma@students.iitmandi.ac.in. 4.—e-mail: sumeetshrm8@gmail.com

We report electromagnetic radiation (EMR) detection from Soft PZT (SP-5A) under impact at low temperature (300–203 K). EMR from our sample was detected by a copper loop antenna placed around the sample. We found that EMR amplitude decreases with lowering the temperature at which the sample was placed. Low temperatures restrict the domain wall motion, due to which dipole movement becomes hindered, which hampers the movement of the charges. Reduced acceleration of charges under impact corresponds to the reduced amplitude of the EMR signals. EMR voltage decreases from 68 V to 21 V as temperature decreases from 300 K to 203 K. The average EMR energy release rate shows a smoothly declining pattern with the decrease in the sample temperature, as well as in hf/kT. EMR detection was made by elastically deforming the samples. Significant EMR voltage even at adverse operating temperatures suggests potential of these materials and this technique for structural health monitoring.

Key words: Electromagnetic radiation (EMR), soft PZT, low temperature, impact loading

INTRODUCTION

Structural health monitoring, a damage identification technique through continuous monitoring of a system, has emerged as a growing research area.[1] Electromagnetic emissions detection is one of the techniques available for structural health monitoring.[2,3] It has been reported that most of the materials emit electromagnetic radiation when fractured.[4–8] The initial study of electrical effects associated with the plastic deformation was reported on ionic crystals. During experimental studies, increase in ionic conductivity and appearance of an electric potential on the surface of ionic crystals was observed by subjecting the crystals to tensile or compressive loading.[9] Later, electromagnetic emissions from various types of rocks subjected to mechanical loading have been studied extensively to develop earthquake prognosis techniques.[4,7,10,11] Surface oscillation models and dipole oscillation models for the electromagnetic radiation (EMR) emissions from rock fracture have been proposed by a group of authors.[12] Electromagnetic radiation emissions from metals was reported by Misra,[13] who subjected the metals and alloys to tensile loading. A theoretical model has been proposed by Misra et al. suggesting vibration of pinned dislocations as the possible cause of the EMR emissions.[14,15] Elastomers, polymer composites, glass and glass–ceramics have been studied for the deformation induced emissions and were named fractoemissions.[5,16–18] Recently, electromagnetic emissions have been studied in rocks as seismic precursors and in polymers and carbon fibres for damage evolution studies.[19,20] EMR from fracture of coal has also been studied and reported under compression and shear for monitoring of stress state in coal mines.[6,21,22] Construction materials like cement and

mortar have been explored for the associated electrical effects.[23–25]

Piezoelectric materials have found wide usage in active vibration control, active shape control, structural health monitoring, etc.[26–29] Piezoelectric materials have been studied extensively for their varying properties under electrical and/or mechanical loadings by a number of authors.[30,31] Dickinson et al. have reported fractoemissions from PZT during its fracture.[32] Song et al. performed in situ measurement of piezo patches mounted on a concrete specimen to detect crack formation and propagation in concrete.[33] Millett et al. have examined phase changes in Nb and Sn doped PZT due to one-dimensional shock loading.[34] They found that with increasing severity of impact, wave velocity decreases, which is due to ferroelectric (FE) to anti ferroelectric (AFE) phase change. Piezoelectric materials have been explored extensively for energy harvesting applications.[35] Use of piezoelectric materials bonded to the surfaces of structures has been analysed and shown in the literature.[33,36,37] Microwave emissions caused by sharp tungsten indenter on the surface of PZT has also been reported.[38] Hoffmann et al. reported correlation between microstructure, strain behaviour and acoustic emissions from Soft PZT ceramics.[39] Recently Sharma et al. reported the preliminary study of EMR emissions from lead-free piezoelectrics under the application of an alternating electric field and from lead-based piezoelectrics (Soft and Hard PZTs) under impact loading.[40–42]

Literature review suggests that EMR detection studies, except for those on ferroelectric materials, are performed during permanent failure of materials which may not be suitable for continuous monitoring of the structures. On the other hand, electromagnetic radiation detection during elastic deformation can be useful for the continuous monitoring of the structures. Moreover, placement and use of sensors in the structures varies according to the loading and environmental conditions to which structures are subjected. Consideration of environmental conditions is also important for the proper functioning of sensors and for the acquisition of data. At many places around the globe the ambient temperature is below 0°C, so for the monitoring of the structures in those particular regions, actuators and sensors should be studied beforehand for their performance under varying temperatures. Soft PZT has been reported to have good piezoelectric properties, hence in the present work EMR emission from a soft PZT (SP-5A) sample under impact loading at low temperatures was studied. The EMR was measured through a non-contact loop antenna and the results are presented here.

EXPERIMENTATION AND INSTRUMENTATION

Soft PZT (PZT SP-5A) cylindrical samples having diameter and height of 6.35 mm and 15 mm, respectively, purchased from Sparkler Ceramics Pvt. Ltd, Pune, India were used in this study. PZT samples were poled along their largest dimension having silver electrodes on both the opposite faces. Dissipation factor (tan δ), piezoelectric charge constant (d_{33}), and capacitance of the soft PZT were 0.019, 457 pC/N and 36 pF, respectively.

The experimental set up we used to obtain the EMR signals under impact is shown in Fig. 1. Cylindrical samples were placed in between the bakelite plates such that loading is done along the poling axis as shown in Fig. 1. The sample could be tightened between the plates with the attached bolts. The upper bakelite plate had a steel rod rigidly fixed to it. The steel rod had holes with a spacing of 3 cm which was used for dropping the weight (0.5 kg) from desired height using a key. With the removal of the key the weight falls and impacts the sample. The bakelite plates had negligible weight, but could resist the operating temperature and served as insulators at the two ends of the cylindrical ceramic sample. This setup was placed in an environmental chamber (with an operating range of 203 K to room temperature) for conducting the experiments.

For EMR radiation detection, a circular metallic strip of copper was used as an antenna. A rectangular strip of 115 mm × 12 mm was cut from a copper sheet of thickness 0.1 mm and was bent to form a thin loop having height and diameter of 12 mm and 36 mm, respectively. This loop was placed around the sample so that it did not come in contact with the sample surface and served as an antenna. Using a 1 MΩ impedance probe, this antenna was connected to a 250 MHz digital storage oscilloscope (D.S.O) having sampling rate of 2.5 GSa/s. The other end of the probe was connected to ground. The signal detection was done by tuning the oscilloscope to the single shot mode before each test. To get rid of the external electromagnetic noises, experiments were conducted at an isolated place in the laboratory so that the experimental set up (including sample, oscilloscope and loop antenna) remains unaffected by external noise. Noises occurring due to the triboelectric effect due to twisting, flexing and transient impacts on the cable were also checked and found to be negligible.

For calculating the modulus of elasticity (E), strain gauges (5 mm; 120 Ω) were fixed on the sample and strain was recorded by NI 9235 data card. A universal Testing Machine (UTM, Tinius Olsen, H50 KS) with load capacity of 50 kN was used for the application of load on the piezoelectric samples. Liquid Nitrogen was used to maintain the desired low temperature of the environmental
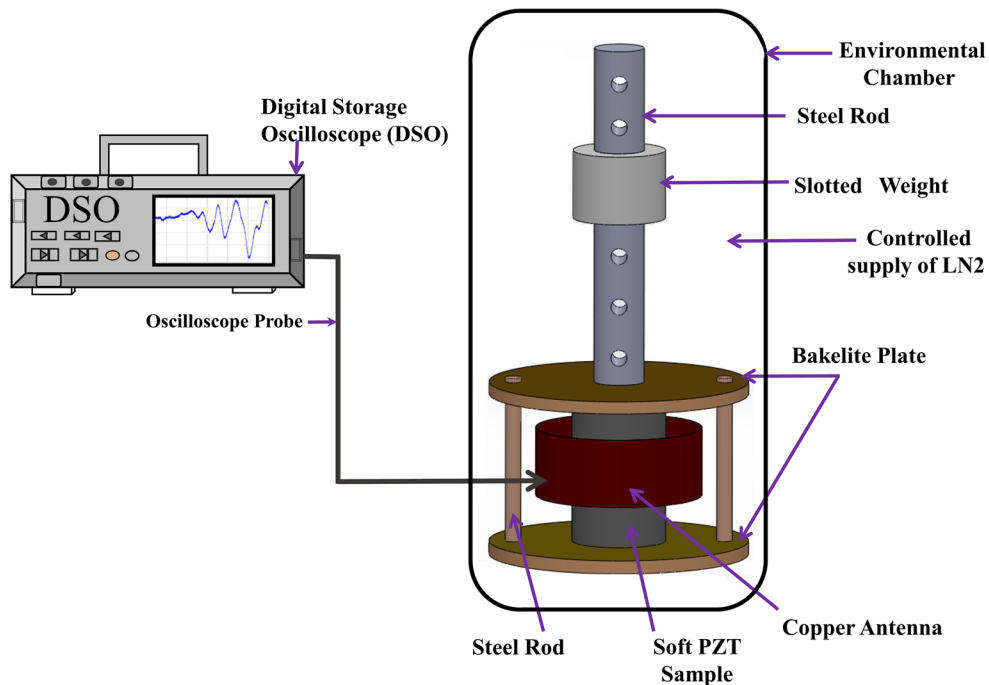
Fig. 1. Schematic diagram of experimental setup.

chamber. The sample was placed in the environmental chamber of the UTM. At the desired temperature, samples were loaded up to 32 MPa (below the elastic limit) and the corresponding stress values (from the UTM) and strain values (from the strain gauge) were used for the calculation of E. Low temperature x-ray diffraction was done using Cu-Kα radiation (Rigaku Smart lab, Rigaku Tokyo, Japan). The pattern was collected in the angular range (2θ) of 10°–90°, with step size of 0.02° in the temperature range of 300–203 K.

RESULTS AND DISCUSSIONS

As shown in Fig. 1, for conducting these experiments, the impact loading setup was placed in the environmental chamber (203–300 K). A slotted cylindrical weight was dropped with the help of a key at a fixed temperature. To learn about the actual behaviour of PZT in terms of practical applications, one PZT sample was used for conducting the experiments over the whole temperature range. Six readings were taken at each temperature on one sample; data showed scatter within 6%, which has been shown with error bar. Figure 2 shows a sample plot of EMR voltage versus time response recorded for the soft PZT at different temperatures for an impact height of 15 cm.

The occurrence of EMR signals from PZT under impact loading can be explained as follows. PZT being ferroelectric in nature contains domains, and for poled sample dipoles in each domain are oriented in the same direction. When an impact load is applied to the piezoelectric material, movement of
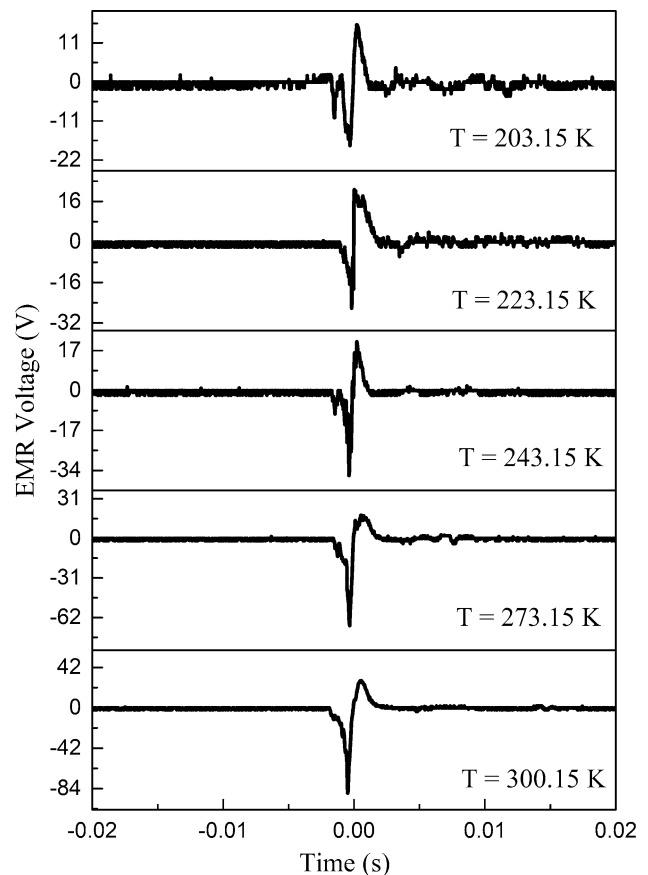

Fig. 2. Sample plot of EMR Voltage–time response for different temperatures for impact height of 15 cm.

charges takes place which consequently gives rise to changes in the surface potential. When PZT is subjected to impact loading up to the elastic limit, it is disturbed from its equilibrium position. The disturbances caused are transient in nature and, due to inertia, the PZT sample again comes to its equilibrium state. The impact loading sets up a time varying deformation wave[43] in the sample, which leads to the change in the dipole moment due to the deformation of the unit cells, which consequently develops the time varying potential across the surface of the sample. Time-varying movement of charge gives rise to electromagnetic waves,[44] thus the time varying change in the dipole moment due to the impact loading gives rise to EMR, which is captured through the copper antenna and is stored in the digital storage oscilloscope (D.S.O). Typical signal plots of EMR at each temperature are shown in Fig. 2. Each signal shows a similar nature with two sharp peaks, one of which is positive and the other is negative. Further, it is observed that the shape of the signal is dependent on the orientation of the placed sample. Figure 3a shows the EMR signal obtained when the positive flat face of the sample is facing the striker. The first peak is observed to be positive followed by a negative peak. However, when the negative side of the sample is facing the striker, the first peak of the obtained signal is negative followed by a positive peak as shown in Fig. 3b. During impact loading the PZT sample deforms, and reorientation of charges causes a change in dipole moment and consequently leads to EMR. Also the impact causes a deformation wave and before attaining equilibrium the material

deformation in the opposite direction also takes place due to inertia and leads to the opposite loop in the signal.

Molecular structure of any material may be affected by variation in temperature and may affect the obtained EMR. To confirm whether any phase change takes place within the temperature range considered, XRD was performed at temperatures ranging from 300 K to 203 K. Figure 4 shows the XRD pattern of soft PZT SP-5A at 300 K and 203 K; remaining XRD patterns are not shown here. Phase transformation studies of PZT at different temperatures with varying mole fractions of $PbTiO_3$ are well reported in the literature.[45] Noheda et al. have studied the tetragonal to monoclinic phase transformations in PZT at low temperatures. Phase transformation from tetragonal to monoclinic has been observed at 20 K.[45,46] In the present study the lowest temperature attained was 203 K (which is far above 20 K), at which no change in XRD pattern was observed and is in line with the literature.

As EMR signals are detected under impact loading, so ferroelastic domain switching or depolarization under impact load also becomes an important parameter to analyse. For this, EMR signals from soft PZT were recorded at room temperature under impact loading (for 150 impacts; H = 15 cm). EMR signals during all the impacts (for the same height of impact) were found to be same with a scatter in data of 4%. This study concludes that impact loading does not depolarize the material, or very high loads are required for depolarizing the PZT. So, the remaining factor is temperature, which can
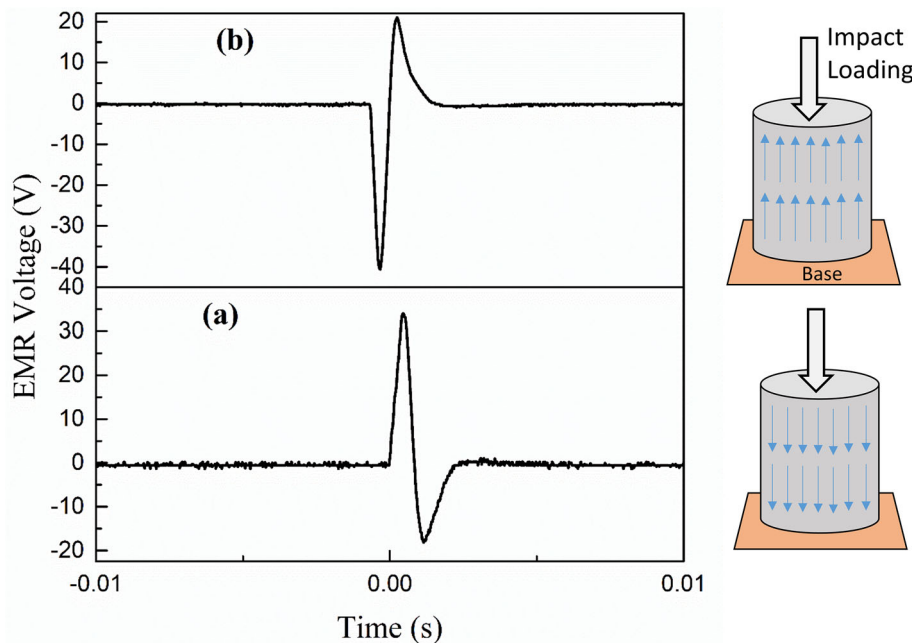

Fig. 3. EMR signal obtained for the impact height of 9 cm (a) when positive flat face of the sample is facing the striker and (b) when negative flat face of the sample is facing the striker.
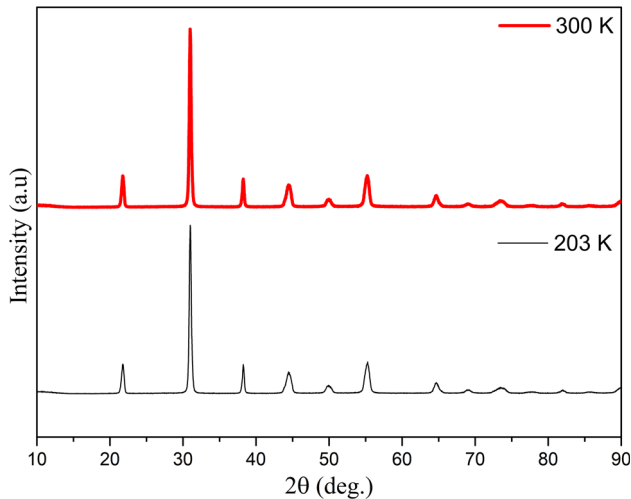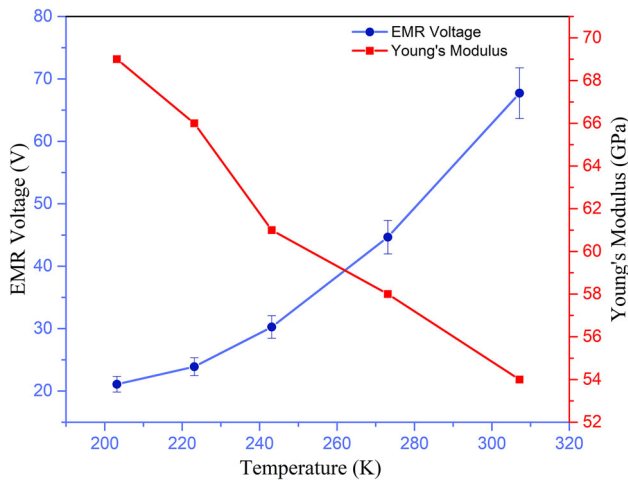
Fig. 4. X-ray diffraction of PZT SP-5A.

Fig. 6. Strain curves for soft PZT loaded up to 50 MPa at 300 K and 203 K.

Fig. 5. Variation of Young's modulus (E) and EMR voltage (V) with change in temperature.

affect the EMR signal and is discussed in the following paragraphs.

As the soft PZT (SP-5A) is tested under impact loading at low temperatures for EMR emissions detection, the elastic modulus (E) becomes an important parameter which can affect the results. So, elastic modulus (E) of the soft PZT was measured at all the temperatures at which the EMR emission detection was conducted. Figure 5 shows the variation of elastic modulus (E) with decrease in the temperature. An increasing pattern can be observed for the Young's modulus (E) with decreases in the temperature. Elastic modulus of the samples was found to be 54 GPa at room temperature, increasing up to 69 GPa at 203 K. Figure 6 shows typical strain curves obtained from soft PZT (using strain gauges) when subjected to compressive loading up to a stress of 32 MPa. Figure 6 shows strain curves of two extreme
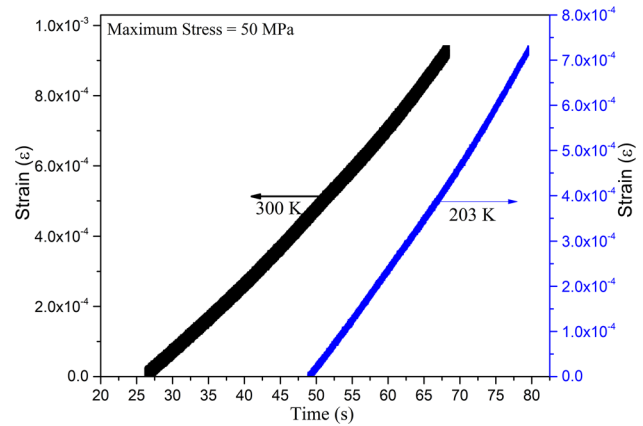
temperatures for better visualisation. Change in slope indicates the increase in stiffness at low temperature, and thereby the increment in Young's modulus.

When ferroelectric ceramics are subjected to external loading, the strain observed in the material has three contributing factors: (1) lattice deformation, (2) domain wall motion and (3) spontaneous domain switching.[47] Among these factors, domain wall motion is the main contributing factor.[47–49] In case of compression, domains switch to the direction perpendicular to the compression axis, whereas in tension domains switch in the direction of the loading axis.[50] Ferroelectric materials have been studied for their ferroelastic behaviour under compressive stress by a number of authors.[47–54] Fett et al. studied the variation of Young's modulus for soft PZT (cylindrical samples) when the load is applied parallel to the poling axis, perpendicular to the poling axis and for the unpoled sample. They concluded that during compressive loading, 90° motion of the dipoles occurs due to which domain wall motion decreases in the direction of the applied stress, while it is enhanced in the direction perpendicular to the applied stress. Moreover, compressive stress allows the movement of domain walls such that the fraction of domains perpendicular to the stress direction increases.[47] Jones et al. measured the extent of domain switching in the cylindrical samples of soft PZT using a neutron diffraction method. They analysed the contribution of ferroelastic domain switching and crystallographic lattice strain in the total strain, and found that macroscopic strain of 0.3% consists of 0.22% ferroelastic domain switching and 0.08% of crystallographic lattice strain.[49] Liest et al. studied the effect of tetragonal distortion (c/a) in La doped bismuth ferrite-lead titanate ceramics at high temperatures, which showed decreasing behaviour (decreases ∼ 10%) and enhanced domain switching. This was also in accordance with reduced energy

barrier for domain switching accompanying increase in temperature.[48]

In the present paper the cylindrical soft PZT (PZT SP-5A) samples were poled along the axis of compression, due to which they showed $E \sim 54$ GPa (Fig. 5) at room temperature and increased with further lowering the temperature. Thus increase in the compression modulus at low temperature can be supported according to the fact that lowering the temperature increases the energy barrier for the domain wall motion, which reduces their motion under compressive stress. As per the discussion, for the strain observed in the ferroelectric sample, domain wall motion is the major contributing factor, decrement of which reduces the strain observed and consequently increases the compression modulus of elasticity (E). Figure 5 shows the variation of EMR signal amplitude with change in temperature. EMR signal amplitude decreases with decreases in the temperature of the soft PZT (SP-5A). Figure 5 shows that for temperatures 300 K, 273 K, 243 K, 223 K and 203 K, EMR voltage was observed to be 68 V, 45 V, 30 V, 24 V and 21 V. The reduction in the amplitude of the EMR signal at low temperature can be supported by the fact that at lower temperatures the domain wall motion is reduced (due to the poling along the compression axis), which causes the reduced motion of the charges within the material. Further increase in Young's modulus (E) with lowering temperature implies a decrease in strain, which aids the reduction of the non-180° motion of dipoles, thus imparting less surface charge. This leads to an overall decrease in the acceleration of dipoles during impact and consequently causes EMR signals with lower amplitudes.

Electromagnetic effects have been reported earlier in many materials under different stimulus conditions, so it is interesting to discuss those along with their proposed genesis for the observed effects. Nitsan has detected electromagnetic emissions from quartz bearing rocks such as tourmaline, sandstone, quartzite, granite etc. during crack propagation and failure.[55] Ogawa et al. detected electromagnetic emissions from different rock samples by hammering, impact loading and during fracture. Ogawa et al. suggested separate electrification (capacitor model) and piezo electrification as the possible source of EM (electromagnetic) emissions.[4] Petrenko et al. tested ice samples under compressive loading for EMR detection. They concluded that charges are induced on the opposite sides of the crack in the ice due to the rupture of interatomic bonds and EMR is consequently emitted.[56,57] Various other authors have also considered charge separation during crack propagation as the possible source of EMR in different materials.[12,18,56–62] In the present case due to the absence of plastic deformation or crack propagation, dislocation formation or rupture of bonds is not happening, thus the existence of dipoles and their response to the impact loading is responsible for the observed EMR

emissions. Electromagnetic radiation emissions during crack formation and propagation can be used in earthquake prognosis, snow avalanche predictions, evaluation of stress state in coal mines etc. The present study is different from the earlier reported studies in the nature of deformation achieved. In this study the samples are elastically deformed for the detection of electromagnetic radiation, which may be useful in the continuous monitoring of structures. For structural health monitoring (SHM), the PZT samples can be embedded in the structures and EMR radiation can be detected, which can represent the state of the structures. Moreover, non-contact radiation detection from PZT may help to get rid of the need for wired networks.

In light of SHM, cement based materials have also been explored for the electrical signals based on the observed piezo effect. Sun et al. studied the piezoelectric effect in cement paste samples by measuring electric current signals under compressive loading of cement.[63] Unlike piezoelectric materials, motion of ions along with water through capillary pores has been suggested as the source of signals. The flow of ions increases with increase in compressive load, which consequently increases the signal amplitude and decreases during the fracture of the specimens.[63] Sklarczyk and Altpeter detected electrical emissions (EE) from mortar and concrete under impact loading. Influence of humidity and the effect of the number of impacts was also analysed. With increase in humidity, EE amplitude decreases and vanishes at R.H > 70%, while an increase in number of blows shows an unpredictable trend.[64] The phenomena observed in cement based materials are mainly attributed to the water content in the cement, which may vary significantly according to changes in climatic conditions. Low amplitude signals still restrict the immediate applications of capillary-based detection methods. Moreover, in cement based materials, most of the studies consists of electrical emissions detection during crack propagation and failure. On the other hand, in the present study PZT tested under elastic limit emits signals of sufficiently high amplitude which are easily detectable. There have been some studies to explore the piezoelectric behavior of cement based ferroelectric composites by measuring their dielectric properties (such as dielectric constant dielectric loss etc.) and piezoelectric properties (such as piezoelectric charge constant, voltage constant etc.)[40,65–68] which suggests the suitability of mixing PZT with cement to form homogeneous composites. Thus, the present work also opens an avenue for exploring cement based PZT composites for their EMR emissions characteristics to serve as a better technological solution for structural health monitoring.

The total free energy of ferroelectric polycrystalline materials is dependent on (1) bulk free energy, (2) elastic energy, (3) gradient energy
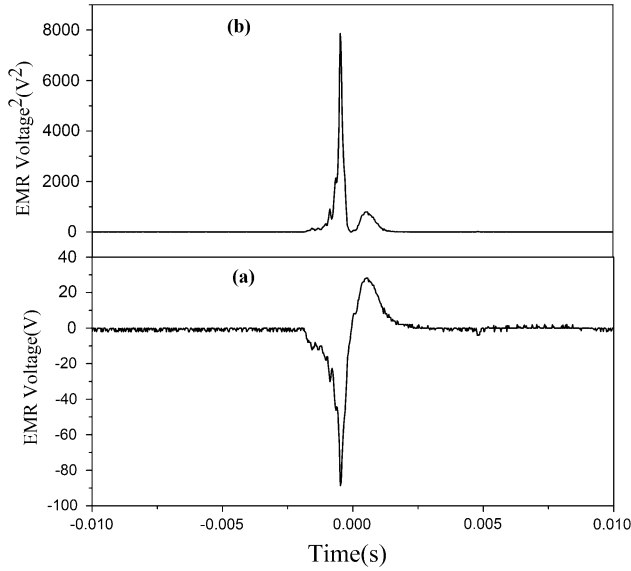
Fig. 7. (a) EMR voltage (*V*)—time (*t*) and (b) EMR voltage square (*V²*)—time (*t*) graph for calculation of average EMR energy release rate at impact height of 15 cm for soft PZT SP-5A.

Fig. 8. Variation of average EMR energy release rate with variation in temperature for impact height of 15 cm.

(which is non-zero only on domain walls and grain boundaries), (4) electrostatic energy and (5) domain wall energy. These factors need to be taken into account when studying the domain switching mechanism in ferroelectric polycrystalline materials.[69,70] In the present case PZT is subjected to impact loading, and acceleration of charges due to the domain switching is responsible for the observed EMR signals. Thus the energy of the EMR signals also becomes an important parameter to be analysed. Moreover, energy is relevant to the transient signals, as is power for the continuous signals. In the present case the observed signals are transient in nature and die out with time, so the recorded EMR signals are used to calculate the EMR energy release rate. Energy of a signal is defined as the square of the amplitude[71] and is calculated for each EMR signal. For the calculation of average EMR energy release rate the $(V - t)$ signal is converted into $(V^2 - t)$ and then the $(V^2 - t)$ curve (shown in Fig. 7) is divided by the time period (t) of the signal, mathematically expressed as:

Average EMR release rate

$$= \frac{\text{Area under the } (V^2 - t) \text{ graph}}{t} = \frac{\int V^2 \mathrm{d}t}{t}. \quad (1)$$

Figure 8 shows the variation of average EMR energy release rate with temperature. EMR energy release rate shows a decreasing trend with decrease in temperature. It varies from 50 V² s/sec to 650 V² s/sec for the temperature ranging from 300 K to 203 K.

EMR voltage which is due to the movement of charges can be related to the piezoelectric charge constant d_{33}. Matthew W. Hooker reported the
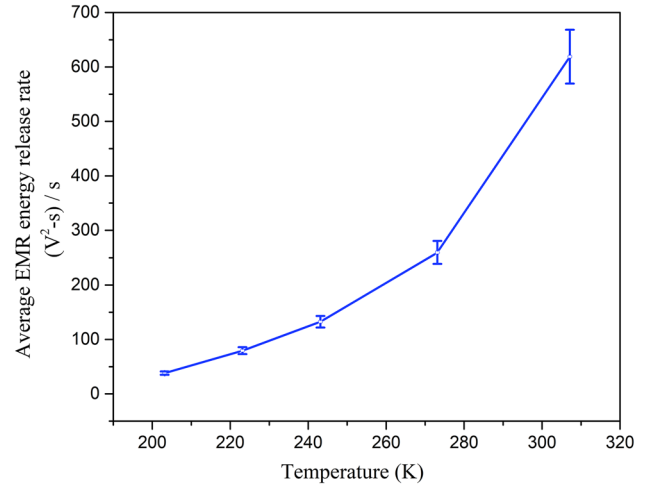
piezoelectric properties of PZT based ceramics between − 150°C to 250°C in which soft PZTs (PZT-5A and PZT-5H) have shown 50% decrease in the d_{33} values.[72] Wang et al. have also studied the influence of temperature on electromechanical and fatigue behaviour of soft PZT (PZT-5H) in the temperature range of − 150°C to 100°C. For the temperature range studied, about 75% decrement in the strain was observed for a given electric field,[73] whereas Zhang et al. observed that d_{33} values decreases from about 245–105 pC/N from 300 K to 10 K.[74] A considerable decrease in the d_{33} values at low temperatures shows that charge developed will be less during impact loading at low temperatures in comparison to that at room temperature, which can be related to the reduced domain switching at low temperatures. Thus EMR voltage which is due to movement of charges shows a decreasing trend with decrease in temperature. FFT (fast Fourier transformation) has been used to calculate the frequency of the observed EMR signals. Variation of EMR energy release rate with the ratio of photon energy (hf) and the thermal energy (kT) (where h = Planck's constant, f = frequency of the signal, k = Boltzmann constant and T = Temperature of the specimen) has been investigated and shown in Fig. 9. It was assumed that EMR energy is proportional to hf, while the thermal energy imparted to the atoms is proportional to kT. The ratio (hf/kT) increases with decrease in temperature, while the average EMR energy release rate decreases. A smooth decreasing pattern of EMR energy release rate is observed with hf/kT as shown in Fig. 9.

According to the present findings, sudden loading on piezoelectric materials is likely to give higher amplitude signals in comparison to gradual loading because the former provides more acceleration of charges, producing higher EMR signals. In practical applications, structures are subjected to varying load conditions[75] and thus, from the SHM point of view, incorporation of these materials into the
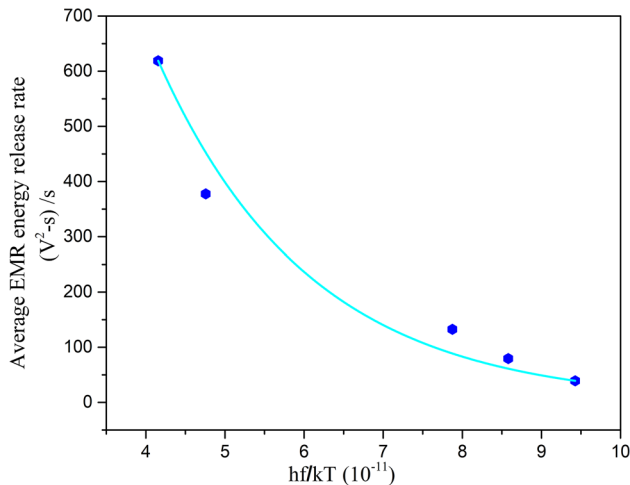
Fig. 9. Variation of average EMR energy release rate with hf/kT.

structure can lead to a way for continuous monitoring of the structures. Thus the deformation induced EMR from piezoelectric materials can be a useful tool for the structural health monitoring.

CONCLUSION

EMR signals from Soft PZT (PZT SP-5A) under the temperature variations of 300 K to 203 K have been investigated. EMR signals show a decreasing pattern with decrease in the temperature. No phase change has been revealed by XRD. So, the decrease in the amplitude of EMR signal under impact at low temperature is due to reduced movement of charges. Young's modulus (E) of PZT shows an increasing pattern from 300 K to 203 K with values ranging from 54 GPa to 69 GPa. Increase in Young's modulus (E) suggests that at low temperatures the movement of domains is hindered, which causes a decrease in the acceleration of moving charges and consequently results in lower amplitude EMR signals. The average EMR energy release rate shows a decreasing pattern with lowering of the testing temperature. Measurement of EMR signals through non-contact techniques under varying temperatures within elastic limits opens up the scope of using these materials for continuous monitoring of structures without any wired networks.

ACKNOWLEDGEMENT

REFERENCES

1. H. Sohn, C.R. Farrar, F.M. Hemez, and J.J. Czarnecki, *Third World Conference on Structural Control*, Como, Italy, April 7–12, 2002, LA-UR-02-2095 (Los Alamos National Laboratory, 2002).
2. M.G.R. Sause, *In Situ Monitoring of Fiber-Reinforced Composites: Theory, Basic Concepts, Methods, and Applications*, vol. 242 (Springer, 2016), pp. 361–456.
3. C. Mavromatou, V. Hadjicontis, D. Ninos, D. Mastrogiannis, E. Hadjicontis, and K. Eftaxias, *Phys. Chem. Earth* 29, 353 (2004). http://hdl.handle.net/11400/15514.
4. T. Ogawa, K. Oike, and T. Miura, *J. Geophys. Res. Atmos.* 90, 6245 (1985).
5. J. Dickinson and L. Jensen, *J. Polym. Sci. Polym. Phys. Ed.* 20, 1925 (1982).
6. G.-J. Liu, C.-P. Lu, H.-Y. Wang, P.-F. Liu, and Y. Liu, *Shock Vib.* 2015, 583862 (2015).
7. V. Frid, *Rock Mech. Rock Eng.* 30, 229 (1997).
8. V. Jagasivamani and K. Iyer, *Mater. Lett.* 6, 418 (1988).
9. A. Stepanow, *Z. Phys. A Hadrons Nucl.* 81, 560 (1933).
10. K. Fukui, S. Okubo, and T. Terashima, *Rock Mech. Rock Eng.* 38, 411 (2005).
11. M. Gokhberg, V. Morgounov, T. Yoshino, and I. Tomizawa, *J. Geophys. Res. Solid Earth* 87, 7824 (1982).
12. A. Rabinovitch, V. Frid, and D. Bahat, *Tectonophysics* 431, 15 (2007).
13. A. Misra, *Nature* 254, 133 (1975).
14. A. Misra, R.C. Prasad, V.S. Chauhan, and B. Srilakshmi, *Int. J. Fract.* 145, 99 (2007).
15. A. Misra, *Appl. Phys. A Mater. Sci. Process.* 16, 195 (1978).
16. J. Dickinson, *Adhesive Chemistry* (Berlin: Springer, 1984), p. 193.
17. J. Dickinson, L. Jensen, and A. Jahan-Latibari, *J. Mater. Sci.* 19, 1510 (1984).
18. Y. Enomoto and M.M. Chaudhri, *J. Am. Ceram. Soc.* 76, 2583 (1993).
19. A. Carpinteri and O. Borla, *Eng. Fract. Mech.* 177, 239 (2017).
20. S. Gade and M. Sause, *J. Nondestr. Eval.* 36, 9 (2017).
21. E. Wang, H. Jia, D. Song, N. Li, and W. Qian, *Int. J. Rock Mech. Min. Sci.* 70, 16 (2014).
22. L. Yavorovich, A. Bespal'ko, P. Fedotov, and A. Popelyaev, *IOP Conference Series: Materials Science and Engineering* (Bristol: IOP Publishing, 2015), p. 012055.
23. M. Cabeza, P. Merino, X. Nóvoa, and I. Sánchez, *Cem. Concr. Compos.* 25, 351 (2003).
24. A. Kyriazopoulos, C. Anastasiadis, D. Triantis, and C. Brown, *Constr. Build. Mater.* 25, 1980 (2011).
25. S. Wen and D. Chung, *Cem. Concr. Res.* 32, 1429 (2002).
26. A. Sharma, R. Kumar, R. Vaish, and V.S. Chauhan, *Int. J. Appl. Ceram. Technol.* 12, E64 (2015).
27. A. Sharma, R. Kumar, R. Vaish, and V.S. Chauhan, *Ferroelectrics* 478, 140 (2015).
28. A. Sharma, R. Kumar, R. Vaish, and V.S. Chauhan, *J. Intell. Mater. Syst. Struct.* 25, 1596 (2014).
29. A. Sharma, R. Kumar, R. Vaish, and V.S. Chauhan, *Compos. Struct.* 128, 291 (2015).
30. D. Zhou and M. Kamlah, *Acta Mater.* 54, 1389 (2006).
31. H. Wang and R.N. Singh, *J. Appl. Phys.* 81, 7471 (1997).
32. J. Dickinson, L. Jensen, and W.D. Williams, *J. Am. Ceram. Soc.* 68, 235 (1985).
33. G. Song, H. Gu, Y. Mo, T. Hsu, and H. Dhonde, *Smart Mater. Struct.* 16, 959 (2007).
34. J. Millett, N. Bourne, and D. Deas, *J. Phys. D Appl. Phys.* 40, 2948 (2007).
35. S.R. Anton and H.A. Sodano, *Smart Mater. Struct.* 16, R1 (2007).
36. C. Soh, K.K. Tseng, S. Bhalla, and A. Gupta, *Smart Mater. Struct.* 9, 533 (2000).
37. S. Bhalla and C. Kiong Soh, *Earthq. Eng. Struct. Dyn.* 32, 1897 (2003).
38. A. Aman, S. Majcherek, S. Hirsch, and B. Schmidt, *J. Appl. Phys.* 118, 164105 (2015).
39. M.J. Hoffmann, M. Hammer, A. Endriss, and D. Lupascu, *Acta Mater.* 49, 1301 (2001).
40. S.K. Sharma, V.S. Chauhan, and A. Kumar, *J. Alloys Compd.* 662, 534 (2016).
41. A. Kumar, V.S. Chauhan, S.K. Sharma, and R. Kumar, *Ferroelectrics* 510, 170 (2017).

42. S.K. Sharma, V.S. Chauhan, and C. Yadav, *Mater. Today Commun.* 14, 180 (2018).
43. W.T. Thomson, *Vibration Theory and Applications* (Upper Saddle River: Prentice-Hall, 1965).
44. D.J. Griffiths and R. College, *Introduction to Electrodynamics* (Upper Saddle River: Prentice Hall, 1999), p. 609.
45. B. Noheda, D. Cox, G. Shirane, J. Gonzalo, L. Cross, and S. Park, *Appl. Phys. Lett.* 74, 2059 (1999).
46. B. Noheda, J. Gonzalo, L. Cross, R. Guo, S.-E. Park, D. Cox, and G. Shirane, *Phys. Rev. B* 61, 8687 (2000).
47. T. Fett, D. Munz, and G. Thun, *Ferroelectrics* 274, 67 (2002).
48. T. Leist, K.G. Webber, W. Jo, T. Granzow, E. Aulbach, J. Suffner, and J. Rödel, *J. Appl. Phys.* 109, 054109 (2011).
49. J.L. Jones, M. Hoffman, and S.C. Vogel, *Mech. Mater.* 39, 283 (2007).
50. T. Fett, S. Muller, D. Munz, and G. Thun, *J. Mater. Sci. Lett.* 17, 261 (1998).
51. A.B. Schäufele and K. Heinz Härdtl, *J. Am. Ceram. Soc.* 79, 2637 (1996).
52. R. Herbiet, U. Robels, H. Dederichs, and G. Arlt, *Ferroelectrics* 98, 107 (1989).
53. G. Arlt, H. Dederichs, and R. Herbiet, *Ferroelectrics* 74, 37 (1987).
54. H. Cao and A.G. Evans, *J. Am. Ceram. Soci.* 76, 890 (1993).
55. U. Nitsan, *Geophys. Res. Lett.* 4, 333 (1977).
56. D. Fifolt, V. Petrenko, and E. Schulson, *Philos. Mag. B* 67, 289 (1993).
57. V. Petrenko, *Philos. Mag. B* 67, 301 (1993).
58. P. Koktavy, J. Pavelka, and J. Sikula, *Meas. Sci. Technol.* 15, 973 (2004).
59. S.G. O'Keefe and D.V. Thiel, *Phys. Earth Planet. Int.* 89, 127 (1995).
60. V.F. Petrenko, *Electromechanical Phenomena in Ice*, DTIC Document (1996).
61. Y. Mizuno and T. Mizuno, *Jpn. J. Appl. Phys.* 41, L209 (2002).
62. S.G. O'Keefe and D.V. Thiel, *J. Electrostat.* 36, 225 (1996).
63. M. Sun, Z. Li, and X. Song, *Cem. Concr. Compos.* 26, 717 (2004).
64. C. Sklarczyk and I. Altpeter, *Scr. Mater.* 44, 2537 (2001).
65. A. Chaipanich, *Curr. Appl. Phys.* 7, 537 (2007).
66. R. Rianyoi, R. Potong, N. Jaitanong, R. Yimnirun, and A. Chaipanich, *Appl. Phys. A* 104, 661 (2011).
67. C. Xin, H. Shifeng, C. Jun, and L. Zongjin, *J. Appl. Phys.* 101, 094110 (2007).
68. Z. Li, B. Dong, and D. Zhang, *Cem. Concr. Compos.* 27, 27 (2005).
69. S. Choudhury, Y. Li, C. Krill, and L. Chen, *Acta Mater.* 55, 1415 (2007).
70. A. Achuthan and C. Sun, *J. Appl. Phys.* 97, 114103 (2005).
71. S. Haykin and B. Van Veen, *Signals and Systems* (New York: Wiley, 2007).
72. M.W. Hooker, *Properties of PZT-Based Piezoelectric Ceramics between − 150 and 250 °C*, (NASA/CR-1998-208708, NAS 1.26:208708) (1998).
73. D. Wang, Y. Fotinich, and G.P. Carman, *J. Appl. Phys.* 83, 5342 (1998).
74. Q. Zhang, H. Wang, N. Kim, and L. Cross, *J. Appl. Phys.* 75, 454 (1994).
75. J.P. Lynch and K.J. Loh, *Shock Vib. Dig.* 38, 91 (2006).